Proceedings of the 21st ICSMGE, Vienna, Austria, 14 – 19 June 2026. Pistrol, Adam & Schweiger (eds.)
Published by: ÖGG, Austrian Society for Geomechanics, Salzburg, Austria, ISBN 978-3-9503898-4-5
https://doi.org/10.53243/ICSMGE2026-504

Three-dimensional finite element modelling of TBM-induced pile response using a simplified numerical approach: application to the TULIP project

Hadia Zaiter, Hussein Mroueh
University of Lille, Lille, France, hadia.zaiter@univ-lille.fr

Emmanuel Bourgeois
Université Gustave Eiffel, Marne-la-Vallée, France

ABSTRACT: In 2020, Société du Grand Paris (now Société des Grands Projets) carried out a research project called TULIP in collaboration with Université Gustave Eiffel, ENTPE and the French Centre for Tunnel Studies. The project involved a large-scale experimental study of the effect of TBM passage on existing piles at Aulnay-sous-Bois (France): three piles were loaded and carefully monitored during the passage of an EPB TBM, and surface displacements were also measured. The results provide a good basis for comparing and validating different numerical approaches. Several numerical models have been proposed to reproduce the observed ground and pile response during the TULIP project (Michalski, 2023; Bourgeois et al., 2024), but their performance remains limited. Recently, (Zaiter, Mroueh and Bourgeois, 2024) have proposed the principle of a simplified numerical procedure for modelling TBM tunnelling using FEM under 2D plane strain conditions. The approach was found to be robust and allows the investigation of different aspects of the TBM process. The aim of this communication is to present and test the extension of this model in 3D conditions, for the TULIP case study. In particular, the influence of the following factors is discussed: grout injection parameters, rheological evolution of the grout injected between the lining and the ground, and TBM advance speed.

KEYWORDS: TBM, pile-tunnel interaction, 3D numerical modelling, finite element modelling, grout injection, advance rate.

1 INTRODUCTION

Tunnel excavation in urban areas often raises concerns about the impact on nearby foundations. TBM-induced ground deformations can affect pile-supported structures, making reliable prediction tools essential (Meschke, Nagel and Stascheit, 2011) .The TULIP project, conducted in 2020 on Line 16 of the Grand Paris Express at Aulnay-sous-Bois, studied this issue through a large-scale in-situ experiment involving three instrumented piles subjected to EPBS tunnelling (Mohamad, 2022).

A prediction exercise (Berthoz et al., 2022) revealed large discrepancies among models, highlighting the need for more robust yet practical approaches. While prescribed-strain methods have shown efficiency (Bourgeois et al., 2024), they require volume loss as input, rather than direct TBM parameters, which limit their predictive capabilities. The present study explores an alternative simplified approach based on the application of a reference stress field in a designated "swelling zone" around the tunnel. This method, implemented in the CESAR finite element code and its Python interface CESAR Pilot (CESAR, 2025), enables direct integration of TBM-related input data and provides a practical alternative for simulating pile-tunnel interaction.

Before applying the approach to the TULIP experiment, it was validated on an academic tunnel case by comparison with a conventional stress-relaxation method, which produced very similar ground responses.

The present work focuses on the 3D analysis of the TULIP case study. In addition to reproducing the observed pile responses, it evaluates the influence of two operational parameters: (i) the rheological evolution of the grout injected behind the lining, and (ii) the TBM advance rate.

2 METHODOLOGY OF THE NUMERICAL MODELING

2.1 *Principle of the proposed approach*

To simulate the mechanical effect induced during TBM excavation, a simplified numerical technique was adopted. The core idea consists in applying a predefined reference stress field within a specific zone of the mesh — referred to as the swelling zone — and converting it into an equivalent set of nodal forces. These fictitious loads are distributed simultaneously to the ground and structural elements (e.g., tunnel lining), and allow the model to reproduce, in a simplified yet effective way, various mechanical actions associated with TBM tunnelling.

The combined effects of excavation-induced pressure, shield geometry and length, and annular grout injection are modelled within a single active zone around the tunnel. Specific mechanical properties are assigned to this zone, enabling the combined application of grouting pressure and stress relaxation forces within a consistent and efficient numerical step (see Figure 1).

Despite its simplified formulation, the method remains compatible with standard finite element procedures and can reproduce a wide range of loading conditions. It is particularly useful in TBM applications where the pressure exerted in the annular gap (by mortar or fluid) varies with depth and evolves over time.

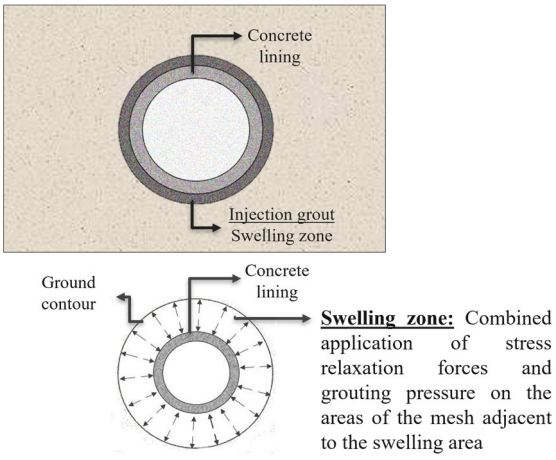

Figure 1. Principle of the swelling model.

2.2 *Implementation in the numerical model*

The approach was implemented in the CESAR finite element code. The loading is defined through a dedicated keyword assigned to groups of elements, where the grout pressure

distribution is specified. The nodal forces corresponding to the difference between the grout pressure and the in-situ stresses are automatically calculated and applied to the boundaries of the swelling zone.

This strategy is efficient, especially in 3D modelling, as it eliminates the need to define the surfaces subjected to the grout pressure (with the right orientation) —often a tedious task in complex or multi-stage models. Rather that explicitly modelling the grout as a material with its own mechanical properties, the swelling zone is represented by a fictitious material with very low stiffness (elastic properties that are not realistic but chosen to serve the purposes of numerical calculations). This allows the imposed pressure to be transmitted directly to the surrounding ground and lining.

2.3 *Definition of the reference stress field*

The reference stress field is defined as the difference between the grout pressure and the initial in-situ stress field. The grout pressure is modelled as a linear function of depth:

$$p = p_{ref} + \gamma(z_{ref} - z) \quad (1)$$

where p_{ref} is the reference pressure (e.g., at tunnel crown depth in this study), γ is the unit weight of the mortar, and z_{ref} is the reference depth.

When tunnelling occurs below the water table, the grout pressure must be written in effective stresses. The hydrostatic pore water pressure is taken as:

$$p_w = \gamma_w(H_w - z) \quad (2)$$

where $\gamma_w$is the unit weight of water and $H_w$is the water table elevation. The effective grout pressure is then obtained by subtracting u_w from the total grout pressure:

$$p = p_{ref} + \gamma_m(z_{ref} - z) - \gamma_w(H_w - z) \quad (3)$$

Rearranging Eq. (3) gives the compact form:

$$p(z) = p_{net} - \gamma'_m z \quad (4)$$

where $p_{net} = p_{ref} + \gamma_m z_{ref} - \gamma_w H_w$and $\gamma'_m = \gamma_m - \gamma_w$is the buoyant unit weight of the mortar. As a result, the model requires only five input parameters: grout pressure at the crown p_{ref}, depth of the crown z_{ref}, γ_m, $\gamma_w$and H_w.

2.4 *Three-dimensional numerical modelling*

2.1.1. 3D model geometry

The three-dimensional geometry of the model was constructed based on the data provided by the TULIP experimental project. A presentation of the project and of the results can be found in (Mohamad, 2022).Some of the data collected are available in (Berthoz et al., 2023). Figure 2 shows a top view of the numerical model. The tunnel is oriented along the horizontal axis, with the excavation progressing from left to right, corresponding to the positive direction of the x-axis.

The piles (named P1, P2 and P3) are located at different positions relative to the tunnel axis, both longitudinally and transversally. Their transverse coordinates are y_{P1} = 0m, y_{P2} = -7m, and y_{P3} = 10m, while their longitudinal positions along the tunnel axis are x_{P1} = 52m, x_{P2} = 62m, and x_{P3} = 72m.

The tunnel is divided into several excavation rings. Each ring corresponds to a tunnel advancement step of 2m. To optimize computational time, the first two segments were modelled with a length of 4m, while the last eight rings were extended to 5m each.

The cross-sectional layout of the model is shown in Figure 3, highlighting the vertical arrangement of the piles relative to the geotechnical layers and tunnel axis. From top to bottom, the ground profile includes made ground (MG), Saint-Ouen Limestone (subdivides in two sublayers, above and below the water table, denoted by SOLdry and SOLsat), Beauchamp Sands (BS), Marly Limestone (ML), and coarse Limestone (CL). The tunnel was excavated using an earth pressure-balance TBM; the diameter of the cutting wheel is D = 9.87m and the axis depth is 21.5m.

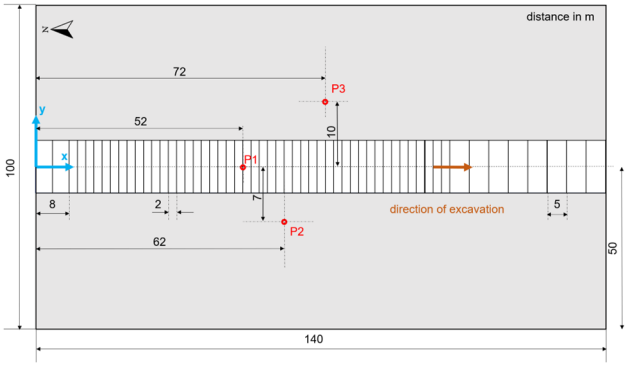

Figure 2. Top view of the numerical 3D model.

The cross-sectional layout of the model is shown in Figure 3, highlighting the vertical arrangement of the piles relative to the geotechnical layers and tunnel axis. From top to bottom, the ground profile includes made ground (MG), Saint-Ouen Limestone (subdivides in two sublayers, above and below the water table, denoted by SOLdry and SOLsat), Beauchamp Sands (BS), Marly Limestone (ML), and coarse Limestone (CL). The tunnel was excavated using an earth pressure-balance TBM; the diameter of the cutting wheel is D = 9.87m and the axis depth is 21.5m.

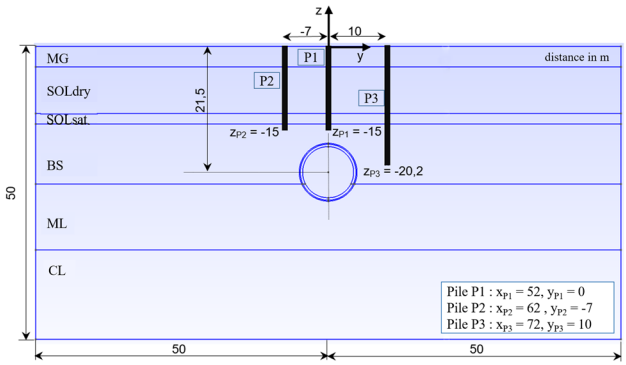

Figure 3. 3D model geometry.

The tunnel crosses the BS and ML layers. Its structure consists of a 40cm thick concrete lining surrounded by a 19cm layer of elements that represents the gap and plays the role of swelling zone in the simulation. The soil inside the tunnel zone corresponds to the local BS and ML strata. Pile P, P2and P3 are modelled with a constant diameter of D_p = 0.5m, with length of L_{P1} = L_{P2} = 15m and L_{P3} = 20.2m.

The model boundaries were defined proportionally to the tunnel diameter D. In the longitudinal direction, the model extends over 14D (140m) to eliminate boundary effects. Transversally, a total width of 10D (100m) was used, and the model depth reaches 5D (50m), sufficient to reach the rigid bedrock at approximately z = -35m, in accordance with the site's geotechnical context.

2.1.2. 3D mesh generation

The three-dimensional mesh was generated using the Python API open-source software GMSH (Geuzaine and Remacle, 2009), which made automation of both geometry creation and mesh generation easier than with the native scripting functionalities of CESAR Pilot, used in previous studies (Klotoé, 2017; Mohamad, 2022). Especially, the GMSH Python API offers greater flexibility and control over the definition of volumes, surface tagging, and mesh structuring. One major

advantage of this approach is the ability to automatically handle volume intersections – such as between piles and soil layers, or between the tunnel lining and the surrounding ground. This capability is enabled by the advance's geometry operations of the OpenCASCADE library.

Figure 4 and Figure 5 illustrate the overall process. The mesh is block-structured, with local refinement around the piles and tunnel to ensure accurate representation of stress and deformation fields in critical zones.

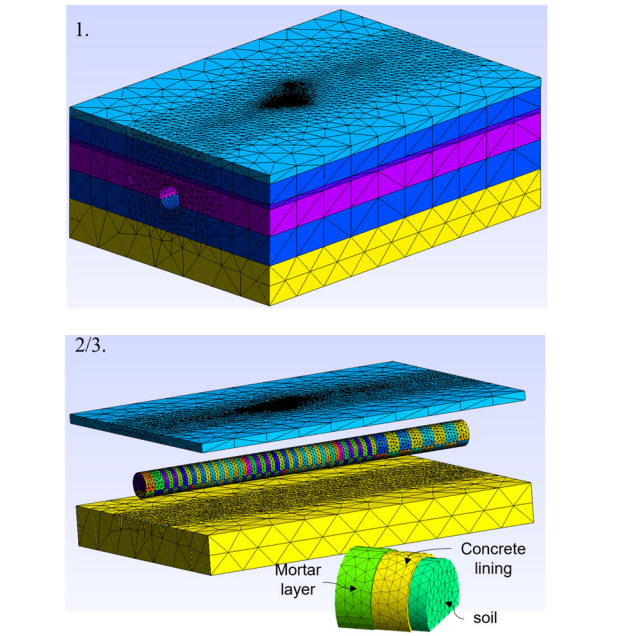

Figure 4. Steps 1 to 4: geometry construction and meshing process

The steps of the mesh generation are as follows: (1) creation of volumetric blocks for the geological soil layers; (2) generation of volumes representing the interior of the tunnel, concrete lining, and mortar layer; (3) division of the tunnel into sequential excavation segments; (4) insertion of piles intersecting the soil layers; (5) detection and removal of overlapping geometries at pile-tunnel-soil interfaces; (6) tagging of physical volumes and surfaces for use in the CESAR input script; (7) application of local mesh size fields, with minimum element size enforced around the tunnel and piles; (8) insertion of zero-thickness joint elements to model the pile-soil interface.

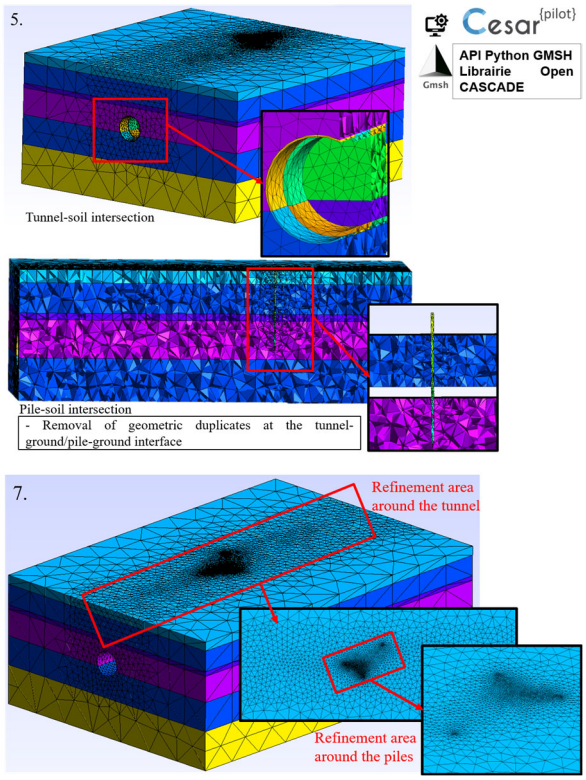

Figure 5. Steps 5 to 7: geometry construction and meshing process

2.1.3. Excavation phasing and numerical procedure

The numerical simulation was structured as a sequence of excavation phases replicating the progressive advancement of the TBM. This phasing was fully automated by a Python script using CESAR Pilot scripting interface.

All the calculations are carried out in drained conditions. The process begins with the initialization of geostatic stresses with $K_0 = 1 - sin\varphi$. A vertical stress of 10 500 kPa is applied at each pile head (equivalent to a vertical load of 2000 kN).

Then, the excavation is simulated through a series of phases indexed from $i = 1\ to\ N + 1$, where N is the total number of excavation rings. At each phase, the excavated segment is updated by assigning the appropriate properties to the tunnel lining (concrete), the annular mortar (based on the proposed approach "swelling model"), and the tunnel interior (soil layers BS o ML, depending on depth). Non-excavated segments retain homogeneous soil properties. Each step also generates a new base file for the subsequent phase.

This automated procedure manages all aspects of the simulation workflow – mesh assignment, material updates, volume activation, load increments, and analysis configuration-ensuring a smooth, continuous, and geomechanically consistent simulation of the TBM advancement. Figure 6 illustrates the full phasing sequence, from initial stress initialization to excavation completion.

2.1.4. Model parameters

The mechanical properties of the soil layers, summarized in Table 1, were taken from (Mohamad, 2022), as defined in a previous benchmark exercise on the TULIP site (Berthoz et al., 2022). In that framework, a detailed geological and hydrogeological characterization was established, and an extensive laboratory and in-situ testing campaign was

performed, including pressuremeter tests in three boreholes, triaxial tests and oedometer tests on samples from each formation. In the present work, no systematic sensitivity analysis was carried out. Regarding boundary conditions, vertical and horizontal displacements were fixed at the base of the model, while horizontal displacements were also constrained on the lateral boundaries.

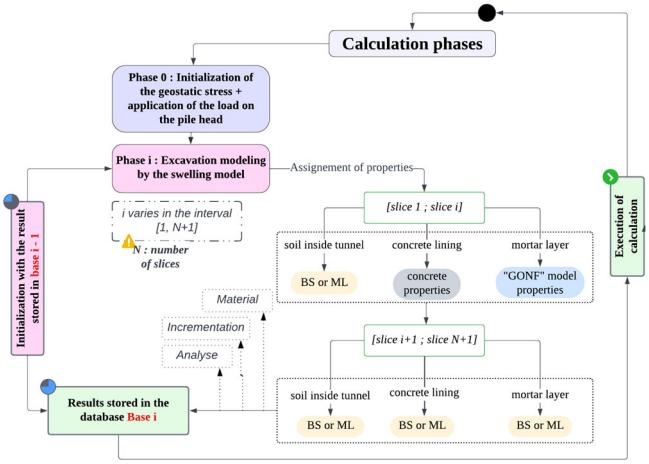

Figure 6. Calculation phases

Table 1. Reference model parameters.

	MG	SOLdry	SOLsat	BS	ML
top of layer (m)	0	-3.5	-11.5	-13.3	-23.5
Unit weight (kN/m³)	19	18	18	21	20
E_{50ref} (MPa)	102	180	327	504	790
E_{uref} (MPa)	307	541	982	1510	2370
p_{ref} (kPa)	17	71	111	142	198
ν	0.3	0.3	0.3	0.3	0.3
c'(kPa)	0	10	10	5	15
φ'(°)	28	33	33	35	38
ψ (°)	0	3	3	5	8
R_f	0.95	0.95	0.95	0.95	0.95
m	0.5	0.5	0.5	0.5	0.5

Following the proposed approach, the properties of the swelling layer (representing the mortar layer) were defined through two consecutive material lines in the dataset introduced by specific keywords, one for the elastic properties, and one for the swelling model. The net pressure $p_{net}$was adjusted so that the computed response reproduces the measured deformations at the TULIP site; the calibrated value corresponds to an injection pressure at the tunnel crown of 58 kPa. The submerged unit weight of the mortar was $\gamma'_m = 12.4\ kN/m^3$.

3 NUMERICAL RESULTS AND INTERPRETATION

The simulations presented below model the interaction between the tunnel and three instrumented piles (P1, P2, P3) using a 3D finite element approach. The analysis includes both the initial loading phase and the sequential excavation stages.

3.1 *Pile response under initial loading*

Figure 7, Figure 8 and Figure 9 present the experimental and numerical results for piles P1, P2, and P3, respectively, after the application of the initial vertical load of 2000 kN. For each pile, two curves are shown: (a) vertical displacement and (b) axial force as a function of depth. Numerical results (P num) are compared against experimental data (P exp).

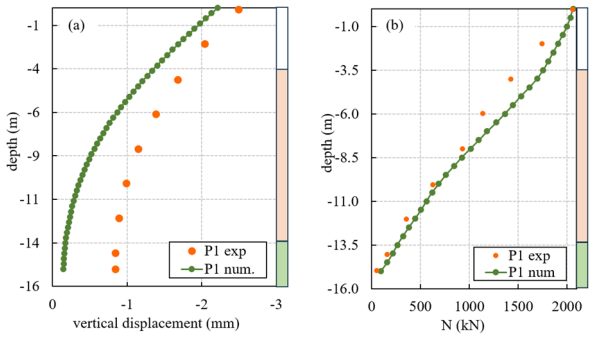

Figure 7. Loading of P1

For pile P1, the vertical displacement decreases progressively with depth, reaching -2.2 mm at the pile head, which closely matches the measured value of -2.5 mm, and becomes negligible at the toe. The axial force exhibits a regular distribution along the pile aligns well with experimental data, particularly between depths of -14 m and -8 m.

For pile P2, the axial force is also well reproduced by the model. However, the settlement at the pile head is underestimated: the simulation yields -2.2 mm versus -3.2 mm measured in the field. Despite having an identical geometry and material properties to P1, the experimental settlements of the two piles differ. Since both piles were modelled with the same parameters, the simulation produces nearly identical responses, failing to capture the observed differences.

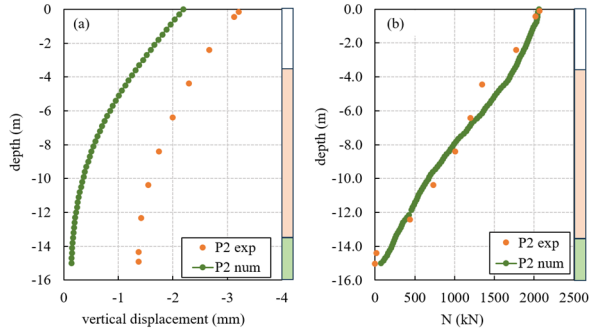

Figure 8. Loading of P2

For pile P3, the numerical and experimental results show good overall agreement. The vertical displacement follows the observed trend, through slightly overestimated at the head (-2.1 mm in the model versus -1.9 mm measured). The axial force, however, is overestimated in the upper layers – particularly in the made ground (MG) and the Saint-Ouen limestone (SOL) – with a deviation of approximately 20% observed around 5m depth.

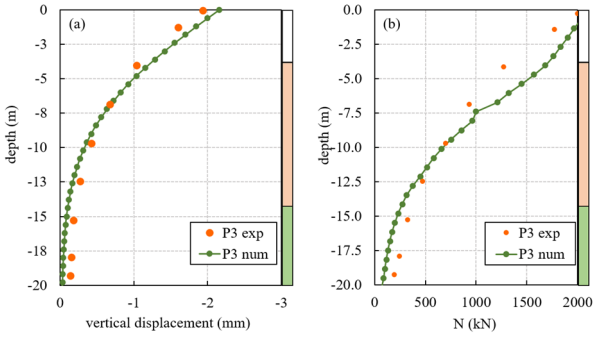

Figure 9. Loading of P3

3.2 *Pile response during excavation*

The following results present include vertical displacements and axial forces profiles for piles P1, P2, and P3.

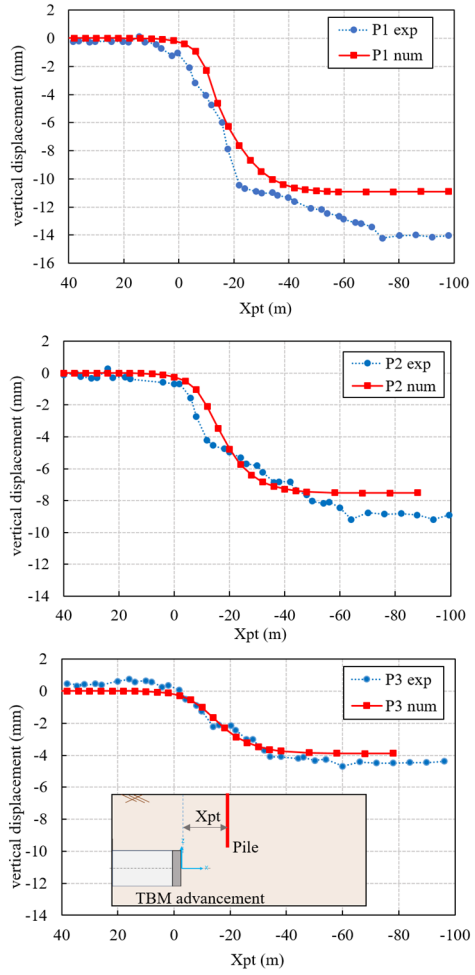

Figure 10. Pile heads settlement vs Xpt (distance between the pile and the cutting wheel): comparison between simulations and measurements

Figure 10 shows the evolution of the pile heads vertical displacements as the TBM advances. For P1, settlements start X_{pt} = 0 m and stabilize near -10.5 mm beyond X_{pt}=-30 m. The simulation closely follows the experimental trend, confirming the pile's sensitivity to TBM-induced ground movements. For pile P2, settlement initiates around X_{pt} = 0 m and stabilizes at approximately -7.5 mm. The simulation captures the shape and magnitude of the experimental curve. Located farther from the tunnel axis, P3 shows reduced impact – settlement reaches only 4.2 mm, with very good agreement between simulation and measurements.

Figure 11 shows the evolution of the axial forces in the piles as the TBM advances. For pile P1, the axial force evolves from about +200 kN to a minimum of -600 kN post-excavation, indicating negative skin friction mobilized by downward soil displacement. The computed profile agrees well with the field data. For pile P2, the axial force increases progressively, peaking at around 600 kN, though the field measurements remain lower, suggesting a moderate overestimation of shaft friction. In pile P3, the axial force increases significantly after excavation, up to 1600 kN, which exceeds experimental values (~800 kN) but maintains a similar trend, reflecting shaft resistance mobilization in deeper layers.

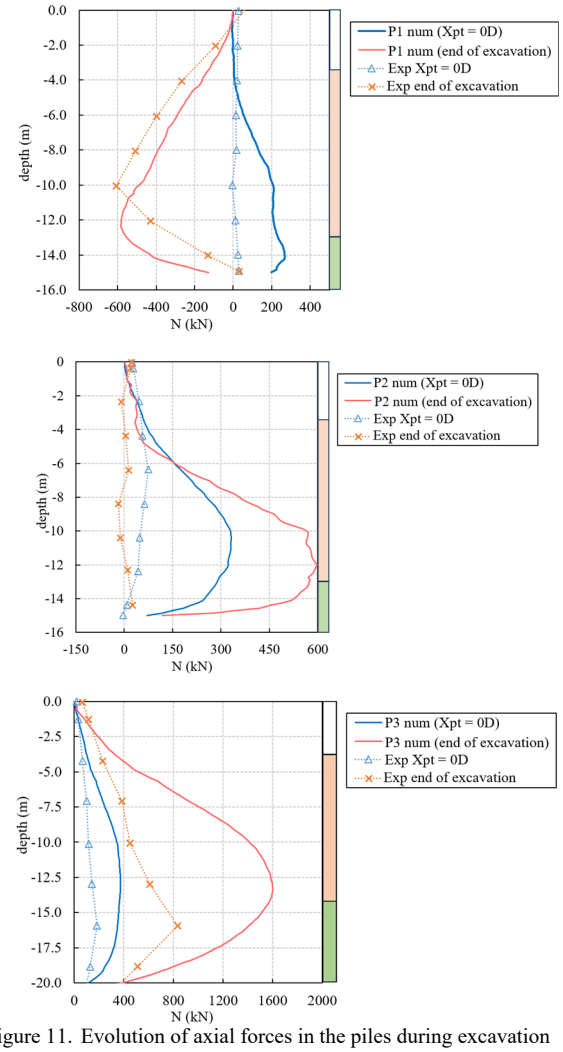

Figure 11. Evolution of axial forces in the piles during excavation

4 PARAMETRIC STUDIES: GROUT RHEOLOGY AND TBM ADVANCE RATE

In this section, simulations with only one pile (P3) are conducted to evaluate the impact of two key parameters: the time-dependent rheology of the mortar and the TBM advance rate. The analysis is focused on the resulting vertical displacements and axial force distributions.

4.1 *Effect of grout rheology on pile response*

To account for the time-dependent hardening of the annular grout layer, the numerical model was modified to include a rheological evolution of its mechanical properties. Specifically, the elastic modulus of the mortar was updated progressively as a function of excavation phases.

The implementation relies on adjusting the material properties assigned to the mortar elements based on the excavation progress. Close to the TBM wheel (slices i-6 to i), the mortar is assigned a swelling-type model; then after a critical number of segments (corresponding to a few days of curing), it is switched to purely elastic model (slices 1 to i-6). A daily advance rate in the TULIP project of 12 m/day was assumed, based on field records during the TULIP project between 29 June to 23 July 2020 (Mohamad, 2022).

Figure 12 presents the numerical results alongside experimental measurements. The left graph shows the evolution of vertical displacement at the pile head as the TBM advances, while the right plot displays axial force distributions with depth.

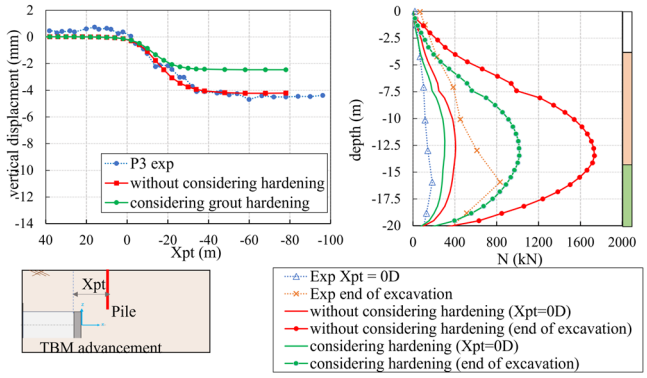

Figure 12. Effect of grout hardening on pile response (pile P3).

Considering grout rheology reduces the computed axial forces and settlements. The head settlement was -4.2 mm in the reference simulation, and -2.5 mm when rheology is considered. The agreement with measures is worse for settlement, but significantly improved for the axial force.

At the end of excavation, the simulation without rheology significantly overestimates the force, reaching about 1700 kN at 13.5 m depth, while the rheological model limits it to approximately 1010 kN – closer to the measured values. This improved agreement, especially in the deeper layers, highlights the importance of accounting for the time-dependent hardening of the grout in realistic pile-tunnel interaction modelling.

4.2 *Influence of TBM advance rate*

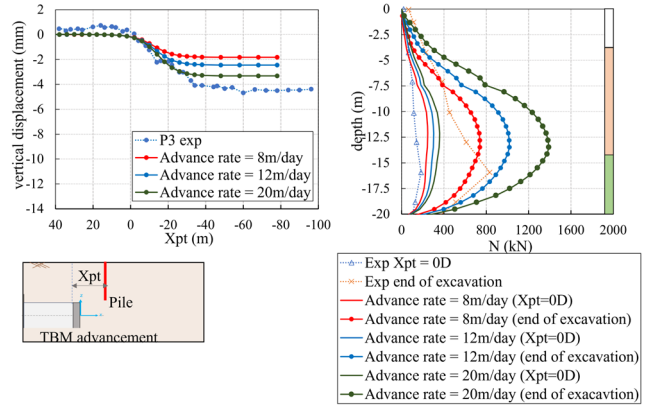

Figure 13. Effect of TBM advance rate on pile P3 response

To evaluate the effect of excavation rate, two additional scenarios were considered by shifting the slice index at which the property change occurs. A slower advance rate of 8 m/day and a faster rate of 20 m/day were simulated .

The results for P3 (Figure 13) highlight a clear sensitively to the TBM advance rate. As the advance rate increases from 8 m/day to 20 m/day, settlement grows from -1.8 mm to -3.3 mm, compared to -4.5 mm measured in the field. Axial forces distributions are plotted both at the end of excavation and at the moment the TBM face reaches the pile location (X_{pt} = 0D), and compared against experimental data (orange and blue dashed lines). At X_{pt} = 0D, all models slightly overestimate the axial force, while final values show a clear increase with TBM speed. The faster the advance, the greater the mobilized shaft friction, particularly in the upper half of the pile.

5 CONCLUSIONS

This study presented a simplified numerical approach to simulate the effects of TBM excavation on pile foundations. The methodology, based on the application of a reference stress field over a “swelling zone”, makes it possible to model TBM-soil-pile interaction in a very simple way, compared with many models found in the literature. The model was first validated against the full-scale TULIP experiment by comparing numerical predictions with measurements on three instrumented piles. The simulations successfully reproduced the evolution of both head settlements and axial forces during TBM advancement.

Parametric studies further demonstrated the influence of grout rheology: accounting for time-dependent hardening significantly reduced overestimated axial forces and better results with experimental data, particularly in deeper sections of the pile. The approach also makes it possible to account for the influence of TBM advance rate: faster excavation rates led to increased settlement and higher shaft friction mobilization, underscoring the importance of considering the evolution of grout hardening in the modelling process.

6 ACKNOWLEDGEMENTSS

Results presented in this paper have been obtained within the framework of the French research Project E-PILOT (Evaluation of the impact on PILes response during Tunnelling) E-PILOT ANR-21-CE22-0011. E-PILOT is a joint industry project dedicated to the behaviour of piles during Tunnelling. The project, driven by University Gustave Eiffel involves 4 contracting or consulting companies of the civil engineering sector, 2 contracting authorities and 4 universities and research laboratories. The project is funded by the partners, ANR (French National Research Agency) and MTE (French Ministry for Ecological Transition).

REFERENCES

Berthoz, N., Bourgeois, E., Branque, D., Michalski, A., Mohamad, W., Le Kouby, A., Szymkiewicz, F. and Kreziak, C., 2022. Impact du creusement au tunnelier sur un pieu : synthèse de l’exercice de prévision TULIP. *Revue Française de Géotechnique*, (173), p.2. https://doi.org/10.1051/geotech/2022015.

Berthoz, N., Branque, D., Michalski, A., Mohamad, W., Bourgeois, E., Le Kouby, A., Szymkiewicz, F. and Rallu, A., 2023. Impact of tunnelling on piles in Parisian subsoil: dataset of in-situ measurements in the ground and on three instrumented piles. *Data in Brief*, [online] 47, p.108971. https://doi.org/10.1016/j.dib.2023.108971ï.

Bourgeois, E., Mohamad, W., Szymkiewicz, F., Le Kouby, A. and Kreziak, C., 2024. Three-dimensional finite element analysis of TBM influence on existing deep foundations: application to the TULIP project. *Geomechanics and Geoengineering*, 20(2), pp.376–389. https://doi.org/10.1080/17486025.2024.2402065.

CESAR (2025) https://cesar.univ-gustave-eiffel.fr

Geuzaine, C. and Remacle, J.-F., 2009. *Gmsh: a three-dimensional finite element mesh generator with built-in pre-and post-processing facilities*. *Int. J. Numer. Meth. Engng*, 79(11), 1309-1331.

Zaiter, H., Mroueh, H. and Bourgeois, E., 2024. Simplified finite element modeling of TBM tunneling. *Proc. XVII European Conferencepo on Soil Mechanics and Geotechnical Engineering*. Lisbon, 967-970.

Klotoé, M.E.C.H., 2017. *Modélisation de l’influence des techniques de présoutènement sur les tassements provoqués lors du creusement des tunnels peu profond*.

Meschke, G., Nagel, F. and Stascheit, J., 2011. Computational Simulation of Mechanized Tunneling as Part of an Integrated Decision Support Platform. *International Journal of Geomechanics*, 11(6), pp.519–528.

Michalski, A., 2023. *Evaluation de l’impact du creusement au tunnelier à front pressurisé sur des fondations profondes*. Thèse de doctorat. Université de Lyon.

Mohamad, W., 2022. *Effet de la construction des tunnels sur les fondations profondes : Cas du Grand Paris Express*. Thèse de Doctorat. Université Gustave Eiffel.